Published in
Journal of Physics B: Atomic, Molecular and Optical Physics 13, issue 6, 1111-1124, 1980
which should be used for any reference to this work

Optical resonances in a strong modulated laser beam

P Thomann†

Laboratoire de Physique Expérimentale, Ecole Polytechnique Féderale, Lausanne, Switzerland

Abstract. The fluorescent intensity of two-level atoms irradiated by a near-resonant amplitude-modulated light wave is calculated in the Bloch model. The analogy with magnetic resonance in a strong oscillating field making an arbitrary angle with the static field is pointed out. Experimental evidence of the predicted parametric and multiple quantum resonances has been obtained with an atomic beam of sodium. Optical pumping was used to prepare the sodium atoms as two-level systems.

1. Introduction

We consider in this paper an assembly of independent two-level atoms irradiated by an intense near-resonant laser beam. The properties of such a system have been thoroughly studied in the case of a constant-amplitude laser beam. The power-broadening of the fluorescent resonance (Citron *et al* 1977), the spectral properties of the re-emitted radiation (Schuda *et al* 1974, Wu *et al* 1975, Hartig *et al* 1976) as well as its statistical properties (Dagenais and Mandel 1978) all reflect in some way the frequency of cycling between ground and excited levels, known as the Rabi frequency.

Here the effect of an additional modulation of the laser field amplitude on the total fluorescent intensity is considered. The laser light contains three spectral components: a carrier of angular frequency ω_L and two sidebands of frequency $\omega_L \pm \omega_1$. We shall use the formal analogy between a two-level system coupled to external fields and a spin $\frac{1}{2}$ in a magnetic field to describe the atom in terms of a pseudo-spin vector (Feynman *et al* 1957, Allen and Eberly 1975). The x and y components stand for the atomic dipole moment and the z component is equal to the atomic inversion. This last component is of special interest since it is directly related to the fluorescent intensity which is proportional to $\frac{1}{2}(z+1)$, the population of the excited state. In a frame of reference which rotates around the z axis at the carrier frequency ω_L of the laser beam, the optical Bloch equations (Allen and Eberly 1975) for the pseudo-spin components read

$$\dot{x} = -\gamma_T x + \alpha y \tag{1a}$$

$$\dot{y} = -\alpha x - \gamma_T y + \Omega(t) z \tag{1b}$$

$$\dot{z} = -\Omega(t) y - \gamma_L (z+1) \tag{1c}$$

where α stands for the laser–atom detuning $(\omega_L - \omega_0)$ and γ_L, γ_T are relaxation rates. For atoms in an atomic beam the only relaxation mechanism to consider is spontaneous

† Present address: JILA, University of Colorado, Boulder, Colo 80309, USA.

emission. The radiative width of the upper level is γ_L; it is also the rate at which the atom is pumped into its ground level ($z = -1$). In optical resonance of a two-level atom, the transverse relaxation rate γ_T is related to the longitudinal one by $\gamma_T = \frac{1}{2}\gamma_L$ (Mollow and Miller 1969). The instantaneous Rabi frequency $\Omega(t)$ is related to the electric dipole matrix element $\boldsymbol{\mu}$ and the electric field of the laser $\boldsymbol{E}(t) = \mathrm{Re}[\boldsymbol{\epsilon}E(t) \exp(\mathrm{i}\omega_L t)]$ as:

$$\Omega(t) = (\boldsymbol{\mu}^* \cdot \boldsymbol{\epsilon})\hbar^{-1}E(t) \qquad \text{with } \boldsymbol{\epsilon}^* \cdot \boldsymbol{\epsilon} = 1. \tag{2}$$

The laser amplitude $E(t)$ is modulated at the frequency ω_1 and the corresponding time dependence of the Rabi frequency is

$$\Omega(t) = \Omega_0 + \Omega_1 \cos \omega_1 t. \tag{3}$$

The transformation to the rotating frame is especially useful in the case of a modulated field since it replaces the three circularly polarised modes (of optical frequencies ω_L, $\omega_L \pm \omega_1$) by a constant field and a single radiation mode which is now linearly polarised and whose frequency lies in the RF range.

The atomic inversion in such a system behaves exactly as the longitudinal component of a magnetic dipole placed in a static field whose x and z components, expressed in frequency units are Ω_0 and α respectively, and an oscillating field $\Omega_1 \cos\omega_1 t$, which is parallel to $0x$.

Depending on the relative orientation of the static and oscillating fields, two types of magnetic resonances have been observed:

(i) When the fields are parallel ($\alpha = 0$) the inversion, which is always negative, shows a resonant *decrease* when the Rabi frequency Ω_0 is a multiple of the RF field frequency. These resonances are known as *parametric resonances* (Favre and Geneux 1964, Aleksandrov *et al* 1964, Polonsky and Cohen–Tannoudji 1965, Chapman and Series 1970).

(ii) When the fields are not parallel ($\alpha \neq 0$) the inversion exhibits a resonant *increase* whenever the condition for single or multiple quantum resonance is met. In the best known but special case where the fields are perpendicular ($\Omega_0 = 0$) the resonance condition is $\alpha = (2n+1)\omega_1$ (odd resonances, Winter 1959). However in the most general geometry ($\alpha \neq 0$, $\Omega_0 \neq 0$), the whole spectrum of multiple quantum resonances is allowed, with the resonance condition becoming $\alpha^2 + \Omega_0^2 = n^2\omega_1^2$ (Wilking 1963, Thomann *et al* 1974, Yabuzaki *et al* 1976).

2. Calculation of the atomic inversion

In order to predict the dependence of the fluorescent intensity (i.e. the atomic inversion) on the various parameters involved, two different methods are used. The most obvious one consists of integrating directly the Bloch equations (1), a procedure that leads to analytical results only under certain restrictive conditions (Armstrong and Feneuille 1975, Feneuille *et al* 1976, McClean and Swain 1976, Thomann 1976, to be referred to as I). We summarise below (§ 2.1) the main results that were obtained for the special case where the carrier frequency is tuned to the atomic transition ($\alpha = 0$) and the laser field has a strong amplitude at all times ($\Omega^2(t) \gg \frac{1}{4}(\gamma_L - \gamma_T)^2$). More details can be found in I.

In the general case ($\alpha \neq 0$) where no analytic integration was found, a second method is used to solve the Bloch equations. By Fourier transforming the time-dependent equations (Fontana and Thomann 1976), one is led to a recurrence relation for the Fourier transform of the inversion, which generates an infinite set of coupled linear equations. A numerical solution can then be obtained by solving the system after truncating it to a suitable size. Although the approximate analytic solution closely matches the results of the numerical computation, the latter are used in all comparisons with experimental curves, because of their broader range of validity.

2.1. Analytic integration

Direct integration of the Bloch equations (1) is possible when the two following conditions are met:

(i) no detuning between atom and laser carrier frequency ($\alpha = 0$)

(ii) strong field at all times; $\Omega^2(t) \gg \frac{1}{4}(\gamma_L - \gamma_T)^2$.

This situation is described in detail in I and only the main features of the result are reported here. Defining $\gamma_\pm = \frac{1}{2}(\gamma_L \pm \gamma_T)$, condition (ii) becomes $\Omega^2(t) \gg \gamma_-^2$. The long-term time-averaged atomic inversion is then given by

$$z_0 = -\frac{\gamma_L}{\gamma_+} \sum_{n=-\infty}^{+\infty} J_n^2\left(\frac{\Omega_1}{\omega_1}\right)\left[1 - \frac{\gamma_-}{\Omega_0}\left(\frac{\Omega_0 - n\omega_1}{\gamma_+}\right)\right]\left[1 + \left(\frac{\Omega_0 - n\omega_1}{\gamma_+}\right)^2\right]^{-1} \tag{4}$$

where J_n is the Bessel function of order n. The atomic inversion displays a resonant behaviour when $\Omega_0 = n\omega_1$, with n an integer. The half-width of all the resonances is γ_+. The amplitude z_{0n} of the nth resonance depends on the modulation depth a defined by

$$a = \Omega_1/\Omega_0$$

according to the relation

$$z_{0n} = \frac{-\gamma_L}{\gamma_+} J_n^2(na) \simeq \frac{-\gamma_L}{\gamma_+}\left(\frac{na}{2}\right)^{2n} n!^{-2} \qquad \text{for } a \leqslant 1. \tag{5}$$

At this point it is worth mentioning that the ratio of the two relaxation rates shows up both in the width and in the amplitude of the resonances, which are equal to γ_+ and proportional to γ_L/γ_+ respectively. The ratio $\gamma_T/\gamma_L = \frac{1}{2}$, which is characteristic of optical resonance in a two-level system, is in contrast with the one generally found in magnetic resonance where the relaxation processes affect both levels in the same way, with the consequence that $\gamma_T \geqslant \gamma_L$. Thus, optical parametric resonances restore a larger portion of the initial inversion than their magnetic counterparts.

The position and widths of the resonances are unaffected by the modulation depth. This property has been justified on the basis of quantum-mechanical arguments (Haroche 1971) as well as classical ones (I).

2.2. Numerical calculation

In the optical Bloch equations (1), the three components of the fictitious spin are replaced by their Fourier transforms defined by

$$z(t) = -\frac{1}{2\pi i}\int_{-\infty}^{+\infty} Z(\omega)\, e^{-i\omega t}\, d\omega. \tag{6}$$

The other components $x(t)$ and $y(t)$ are expressed in a similar way in terms of their transforms $X(\omega)$ and $Y(\omega)$. The following set of linear equations is obtained for the Fourier transforms X, Y, Z:

$$(-\mathrm{i}\omega+\gamma_\mathrm{T})X(\omega)-\alpha Y(\omega)=0 \tag{7a}$$

$$\alpha X(\omega)+(-\mathrm{i}\omega+\gamma_\mathrm{T})Y(\omega)-\Omega_0 Z(\omega)-\tfrac{1}{2}\Omega_1[Z(\omega+\omega_1)+Z(\omega-\omega_1)]=0 \tag{7b}$$

$$\Omega_0 Y(\omega)+\tfrac{1}{2}\Omega_1[Y(\omega+\omega_1)+Y(\omega-\omega_1)]+(-\mathrm{i}\omega+\gamma_\mathrm{L})Z(\omega)=2i\pi\gamma_\mathrm{L}\delta(\omega). \tag{7c}$$

Elimination of X and Y from these equations leads to a recurrence relationship between values of Z taken at five equidistant values of the argument, centred at ω and spaced by the modulation frequency ω_1. For convenience of notation, we denote the shift $p\omega$ of the argument of any function of ω by the subscript p. For example

$$Z_p(\omega)\equiv Z(\omega+p\omega_1) \qquad (p=\text{integer}). \tag{8}$$

The recurrence relation takes the following form:

$$a_{p-1}(\omega)Z_{p-2}(\omega)+b_p(\omega)Z_{p-1}(\omega)+c_p(\omega)Z_p(\omega)+b_{p+1}(\omega)Z_{p+1}(\omega)+a_{p+1}(\omega)Z_{p+2}(\omega)$$
$$=2\mathrm{i}\pi\gamma_\mathrm{L}\delta_p(\omega) \tag{9}$$

where the coefficients are defined by

$$a(\omega)=\tfrac{1}{4}\Omega_1^2 q(\omega) \tag{10a}$$

$$b(\omega)=\tfrac{1}{2}\Omega_0\Omega_1(q(\omega)+q_{-1}(\omega)) \tag{10b}$$

$$c(\omega)=-\mathrm{i}\omega+\gamma_\mathrm{L}+\tfrac{1}{4}\Omega_1^2(q_1(\omega)+q_{-1}(\omega))+\Omega_0^2 q(\omega) \tag{10c}$$

$$q(\omega)=(-\mathrm{i}\omega+\gamma_\mathrm{T})[(-\mathrm{i}\omega+\gamma_\mathrm{T})^2+\alpha^2]^{-1}. \tag{10d}$$

Since equation (9) is valid for any integer value of p, it can be considered as the pth equation of an infinite linear system. This system can be put in matrix form by introducing the pentadiagonal matrix $((A))$ (which contains the a, b and c coefficients of equation (10)) and two vectors (Z) and (δ) with components $Z_p(\omega)$ and $2\mathrm{i}\pi\gamma_\mathrm{L}\delta_p(\omega)$ respectively. The system can then be written as

$$((A))(Z)=(\delta). \tag{11}$$

The formal solution of (11) is then

$$Z(\omega)=\sum_{-\infty}^{+\infty} A_{0k}^{-1}(\omega)2\mathrm{i}\pi\delta_k(\omega). \tag{12}$$

The time-dependent inversion which follows from equations (6) and (12) is given by

$$z(t)=-\gamma_\mathrm{L}\sum_{-\infty}^{+\infty} A_{0k}^{-1}(-k\omega_1)\exp(-\mathrm{i}k\omega_1 t). \tag{13}$$

We finally get for the time-averaged inversion

$$z_0=-\gamma_\mathrm{L}A_{00}^{-1}(0). \tag{14}$$

An approximate value of z_0 can be computed numerically by evaluating the central element A_{00}^{-1} of $((A))^{-1}$.

Using equation (14) the atomic inversion z_0 was calculated numerically as a function of the average Rabi frequency Ω_0 and the detuning α. The result is shown in figure 1.

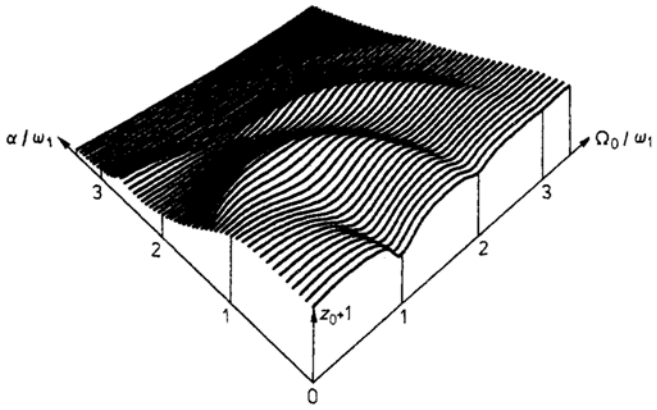

Figure 1. Numerical calculation of the excited state population (z_0+1) as a function of the average Rabi frequency Ω_0 and the detuning $(\alpha=\omega_L-\omega_0)$ for $\gamma_L=2\gamma_T=0{\cdot}2\omega_1$ and $\Omega_1=2\omega_1$.

The modulation amplitude Ω_1 is kept constant rather than the modulation depth $a=\Omega_1/\Omega_0$ in order to show the behaviour of multiple quantum resonances near $\Omega_0=0$. Moreover the modulation amplitude has a larger value $(\Omega_1=2\omega_1)$ than could be attained experimentally, in order to enhance the structure of the surface.

The parametric resonances are characterised by a decrease of the inversion from its saturated value near the Ω_0 axis (for $\Omega_0=n\omega_1$ and $\alpha\simeq 0$). When $\Omega_0=0$, the field geometry in the rotating frame is the same as the one which is common in magnetic resonance, namely a static field along the z axis (its optical analogue is the detuning) and an oscillating field perpendicular to it. Of the resonances at odd multiples of $\omega_1(\alpha/\omega_1=2n+1)$ the first $(n=0)$ is considerably power broadened and the third $(n=1)$, although far from being saturated, shows a sizable power shift.

When neither α nor Ω_0 is zero multiple quantum resonances occur when the total static field is equal, in frequency units, to any integer multiple of ω_1: $((\alpha^2+\Omega_0^2)^{1/2}=n\omega_1)$. The positions of the resonances describe circles in the (α, Ω_0) plane as can be seen in figure 1, although the second resonance is strongly shifted near $\Omega_0=0$ where it vanishes. The three-quantum resonance $(n=3)$ vanishes when $\Omega_0\simeq\omega_1$ (figure 1). This is due to a destructive interference between the four different contributions to the transition probability (Wilking 1963). This phenomenon is an example of a level-crossing of the second kind (Grynberg *et al* 1973) and has been studied experimentally in magnetic resonance (Wilking 1963, Thomann *et al* 1974, Yabuzaki *et al* 1976, Nakayama and Ogawa 1976).

3. Experimental set-up

A schematic diagram of the experimental set-up is illustrated in figure 2. An atomic beam of sodium is illuminated at right angles by two laser beams tuned to the $3^2S_{1/2}$–$3^2P_{3/2}$ resonance line. In order to get rid of the Doppler effect to within the 10 MHz linewidth of the excited level the atomic beam is collimated to 1 mrad by means of two circular apertures which are 20 cm apart. Both the oven and the collimator apertures are 0·3 mm in diameter. Two copper traps, cooled to 77 K, are placed

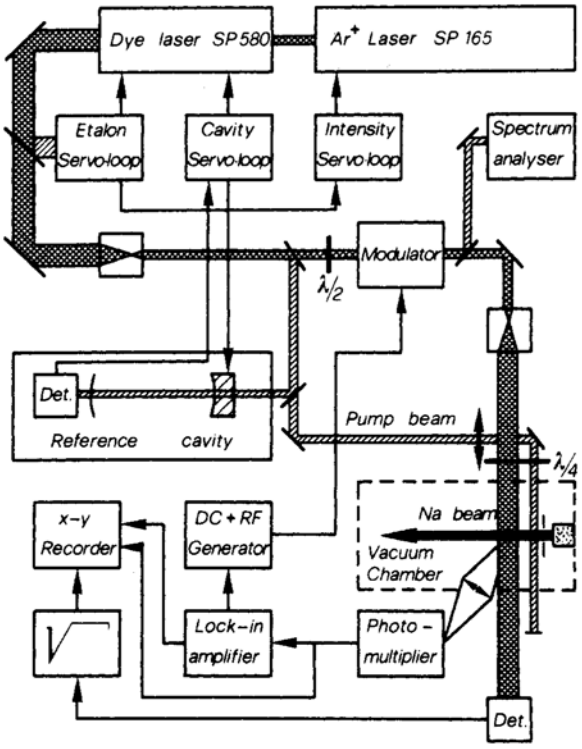

Figure 2. Experimental set-up.

between the two pinholes and close to the interaction region in order to prevent unwanted atoms from reaching it. The dye laser (Spectra-Physics 580) is pumped by the green line of an argon laser (Spectra-Physics 165), and delivers up to 40 mW single-mode power at 589 nm, with an intensity stability of 1%. The short-term frequency jitter was reduced by a factor of two by mechanically isolating the dye cell from the laser cavity. The short term (<20 ms) frequency stability was ±2·5 MHz, which was deduced from the 11·5 MHz minimum linewidth of the low-power resonance fluorescence curves. In order to increase the long-term frequency stability, the laser cavity was locked to a reference cavity (a confocal Fabry–Perot interferometer with a 3 MHz bandwidth). The optical length of the reference cavity was kept constant by placing the cavity in an air-tight cell whose temperature was controlled to within a few thousandths of a kelvin. The overall frequency drift was less than 0·5 MHz/hour. This stabilisation scheme has two advantages over a scheme based on an atomic beam reference. The modulation signal can be applied to the reference cavity instead of the laser cavity, leaving the laser output free from any added modulation. In addition, by adjusting the reference cavity length, the laser frequency can be locked far away from the atomic resonance without any loss in loop gain.

A small fraction of the laser intensity (~1%) is used to prepare the atoms in the desired two-level system by optical pumping (see § 4).

The modulation of the laser beam is achieved by a KD*P transverse electro-optic modulator. The modulation frequency has been chosen so as to allow a reasonable separation of the resonances ($\omega_1/2\pi = 50$ MHz $\gg 10$ MHz $= \gamma_L/2\pi$). Higher modulation frequencies cause heating of the crystal and of the index matching fluid, leading to

serious beam degradation. Even at the frequency used in the experiment, there is a critical trade off between modulation depth and beam quality. The RF voltage that drives the modulator is chopped at 1 kHz in order to improve the detection sensitivity and reduce the power dissipated in the modulator.

The laser intensity is scanned by rotating a half-wave plate between two crossed polarisers which are placed in front of the modulator.

The fluorescent intensity is collected at right angles to both the atomic and the laser beams. Special care is taken to view only that part of the interaction region where the beam intensity is the most homogeneous. To this end, the interaction region is imaged by the collecting optics on a slit parallel to the laser beam, selecting a slice less than 0·2 mm thick in the 0·3 mm diameter atomic beam. The laser beam diameter is typically 2 mm between $1/e^2$ intensity points, resulting in a theoretical homogeneity of 1% for the electric field in the observed region. At high modulation depths, however, the homogeneity was affected by the thermal lensing effects in the modulator. The fluorescent intensity is proportional to the population of the upper state, which is equal to $\frac{1}{2}(z+1)$. Because the light modulation is turned on only half of the time, the photomultiplier current contains a DC component which is proportional to the average fluorescence ($\frac{1}{2}(z_m+1)=\frac{1}{2}[\frac{1}{2}(z(0)+z(a))+1]$) and an AC component at the chopping frequency. The AC component is proportional to the differential fluorescence ($\Delta z = z(0)-z(a)$) and is detected by a lock-in amplifier.

A voltage proportional to the Rabi frequency Ω_0 is obtained by measuring the total intensity of the laser beam with a photocell intercepting the main beam after the interaction region. The output of the photocell is fed into an analogue square-root circuit. The photocell measures the average intensity of the modulated beam, which is proportional to the square of the Rabi frequency Ω_0 multiplied by a form factor which depends on the modulation depth. This form factor is nevertheless independent of Ω_0 and it does not affect the linearity of the amplitude scans.

4. Two-state preparation

Because of hyperfine structure and Zeeman degeneracy, the resonance line of atomic sodium is far from the two-level atom for which the theoretical calculations were made. We use here a simple method to prepare the sodium atoms as a two-state system. The principle was first suggested as part of a three-step procedure (Abate 1974), but the following single-step method has proven perfectly satisfactory (Thomann 1975, Hartig *et al* 1976, Wu *et al* 1976). Although the laser can be tuned selectively to any of the hyperfine components of the resonance line, only two pairs of hyperfine levels can be considered as two-level systems, to the extent that they are free from hyperfine pumping. These pairs of levels are $3^2S_{1/2}$, $F=1$–$3^2P_{3/2}$, $F'=0$ and $3^2S_{1/2}$, $F=2$–$3^2P_{3/2}$, $F'=3$. (In the following, primed quantum numbers refer to the $3^2P_{3/2}$ excited term and unprimed numbers refer to the $3^2S_{1/2}$ ground term.) The $F=2$–$F'=3$ line is in turn made up of several Zeeman components which are superimposed in zero magnetic field but have different electric dipole matrix elements. This means that the evolution in a strong field will involve several Rabi frequencies.

By irradiating the atomic beam with circularly polarised light, optical pumping of the Zeeman states brings all atoms into the two states $F=2$, $m_F=2$ and $F'=3$, $m'_F=3$, which constitute a very good approximation to a two-level system. The $F'=3$, $m'_F=3$ state has only one decay channel, which makes further optical pumping impossible; this

is not true for the $F'=0$ state. Furthermore, the $\Delta m_F = 1$ selection rule for circularly polarised light prevents all transitions from the $F=2, m_F=2$ state to any state belonging to the $F'=2$ and $F'=1$ levels. From any other ground state ($F=2, m_F \neq 2$) such unwanted transitions are possible provided that the power broadening of the $F=2$–$F'=3$ resonance line becomes comparable with the hyperfine splitting of the excited levels; this condition is already met for moderate powers since the $F'=2$ and $F'=1$ levels are separated from the $F'=3$ level by only 60 MHz and 95·5 MHz, respectively.

In order to avoid variations of the pumping efficiency when scanning the laser intensity, and also to reduce spurious hyperfine pumping by the low-frequency sideband of the modulated beam, the two-state preparation is achieved by means of an auxiliary laser beam which is parallel to the main one. The pumping region is 5 mm ahead of the interaction region. The pumping beam is given a $2 \times 0{\cdot}5$ mm^2 section by a cylindrical lens and its intensity is well over saturation (the saturation threshold is defined by the relation $\Omega_0 = \gamma_L$; for the two-state transition considered, it is reached when the laser intensity is equal to 12·6 mW cm^{-2}). In order to prevent mixing of the Zeeman states within a hyperfine level, the two components of the Earth's magnetic field which are perpendicular to the laser beam must be cancelled. With these conditions the pumping process leads virtually all atoms into the two-level system. When the laser is tuned to the two-state transition, the pumping efficiency is limited only by the purity of the circular polarisation.

The upper state of the two-level system is the only one to decay by emitting pure σ^+ radiation. In our detection geometry, σ^+ (and σ^-) radiation appears linearly polarised along the atomic beam, whereas π radiation is polarised along the laser beam. The efficiency of the two-state preparation can thus be checked by measuring the degree of polarisation of the fluorescent light. The effect of hyperfine and Zeeman pumping by the pumping beam can be seen in figure 3 where the fluorescence from the interaction

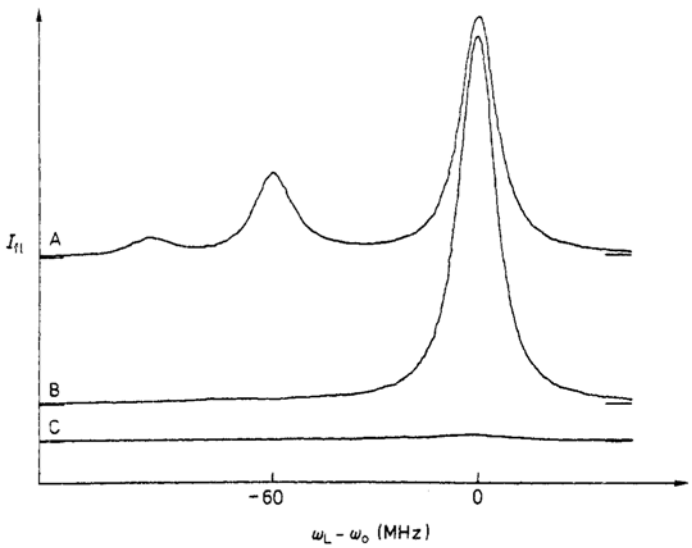

Figure 3. Resonance fluorescence of the $3^2S_{1/2}, F=2$ to $3^2P_{3/2}, F'=1, 2, 3$ transitions versus laser detuning from the two-level frequency separation. Laser intensity = 0·1 mW cm^{-2}, σ^+ polarised without pumping beam (curve A), with pumping beam, σ detection (curve B) and with pumping beam, π detection (curve C).

region is recorded as a function of the detuning of both laser beams from the two-state transition. All three curves were recorded with a low-intensity main beam, with the maximum fluorescence 40 times lower than the saturated fluorescence, such that its pumping action is almost negligible. Both the pumping and main beam are circularly polarised. For reference, curve A shows the spectrum obtained without the pumping beam. The two lower curves are with the pumping beam, and detection polarised along the atomic beam (curve B) and along the laser beam (curve C). Since both the pumping beam and the main beam have the same frequency, the disappearance of the peaks corresponding to the $F = 2\text{–}F' = 2$ and $F = 2\text{–}F' = 1$ transitions is entirely due to hyperfine pumping in the pumping region. The efficiency of the two-state preparation is measured by the degree of polarisation of the fluorescent light, which is equal here to 0·985. When taking into account the degradation of the polarisation due to aperture effects, the remaining unpumped atoms account for 1% of the observed atoms. The height of the peak corresponding to the $F = 2\text{–}F' = 3$ transition increases from curve A to curve B. This is due to the two-state transition having the strongest dipole moment ($\mu = 2{\cdot}52\, ea_0$) of all the σ^+ Zeeman transitions.

5. Experimental results

5.1. Parametric resonances; laser tuned to the atomic transition ($\alpha = 0$)

Figure 4 shows the variation of the fluorescent intensity as a function of the average Rabi frequency Ω_0. The upper curve is the average fluorescence. The fluorescent light increases towards saturation (zero inversion) as long as $\Omega_0 \lesssim \gamma$. The dips at $\Omega_0 = \omega_1$ and $\Omega_0 = 2\omega_1$ are the first two parametric resonances. The lower curve is the differential fluorescence, which is twice the difference between the average fluorescence (upper curve) and the simple inverted Lorentzian which is obtained without modulation (not shown). The dotted line is the corresponding theoretical curve. Since the calibration of the Rabi frequency in terms of the measured laser intensity was not accurate to better

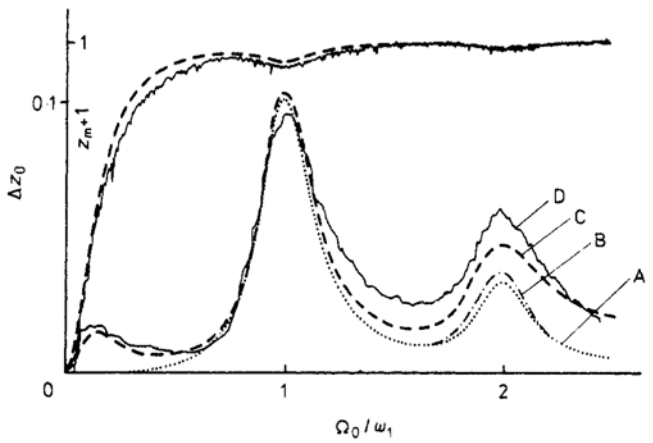

Figure 4. Fluorescence of the two-level at exact resonance versus average Rabi frequency (modulation depth $a = 0{\cdot}58 \pm 0{\cdot}06$); upper curves: average fluorescence (theory and experiment), lower curves: differential fluorescence (curves A–C: theory—see text, curve D: experiment).

than 20%, the horizontal scale of the theoretical curves was adjusted to match the position of the observed resonances. The vertical scale was determined from the saturated DC fluorescence. No further adjustment was made for the differential fluorescence, nor for the width of the resonances. The differential fluorescence signal (curve D) shows a background which increases with Ω_0 and with the modulation depth. On the basis of this dependence the following contributions to the background have been identified.

(i) The non-linearity of the modulator transmission curve (laser amplitude versus applied voltage) results in a small modulation of Ω_0 at the chopping frequency. This modulation is responsible for a spurious peak in the differential fluorescence when the fluorescence is most strongly dependent on Ω_0 (i.e. when $\Omega_0 \leqslant \gamma$, see curve C).

(ii) The non-linearity of the modulator also produces modulation at twice the desired frequency. This modulation generates its own spectrum of parametric resonances (at $\Omega_0 = 2\omega_1$), but this effect is small (curve B includes both the second resonance of the ω_1 modulation and the first resonance of the $2\omega_1$ modulation).

(iii) It was found that the hyperfine pumping of the residual unpumped atoms by the low-frequency sideband of the modulated light can contribute significantly to the differential fluorescence. An estimate of this effect, combined with the two other known sources of error, results in the corrected theoretical curve C. Although a better agreement is found for lower modulation depths a, this curve ($a = 0{\cdot}58 \pm 0{\cdot}06$) is shown here for its clear evidence of the second parameteric resonance, whose amplitude is predicted to vary as a^4 (see equation (5)).

That the agreement is closer for small modulation depths is also illustrated in figure 5 which shows the dependence of the amplitude of the first resonance z_{01} on the modulation depth a. The theoretical amplitude is given by $\frac{4}{3} J_1^2(a)$ (full line, equation (5)), which is approximately quadratic in a over the range considered.

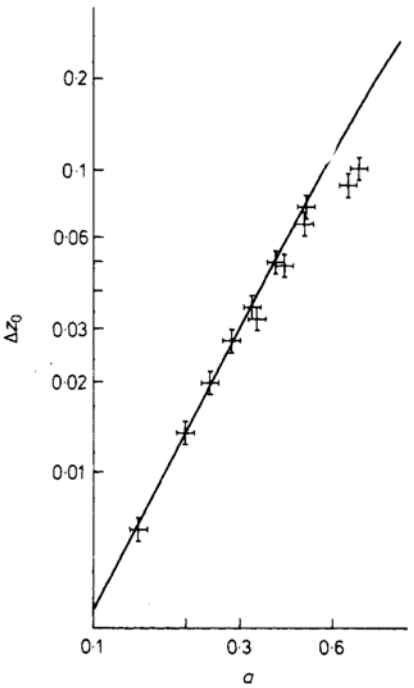

Figure 5. Amplitude of the first parametric resonance ($\Omega_0 = \omega_1$) versus modulation depth a. The theoretical curve is given by equation (5).

5.2. *Parametric resonances; effect of detuning*

The gradual transition from parametric resonances to standard (single and multiple quantum) resonances is shown in figure 6. Here the modulation depth is smaller than in figure 4 ($a = 0{\cdot}35 \pm 0{\cdot}04$) and only the differential fluorescence shows significant structure. Again the horizontal scale is adjusted and the vertical calibration is provided by the saturated DC fluorescence. The theoretical curves are given, as for curve A, figure 4, by the numerical computation (Fourier method), with no correction for the background. Parametric resonances are clearly distinguished from standard resonances: the latter tend to bring the atom closer to saturation (Δz_0 decreases) whereas the former bring the atom closer to its ground state (Δz_0 increases). The position of the nth standard resonance is given by $\Omega_0 = (n^2\omega^2 - \alpha^2)^{1/2}$. The power shift is negligible for this small modulation depth, but the shape of both the standard and

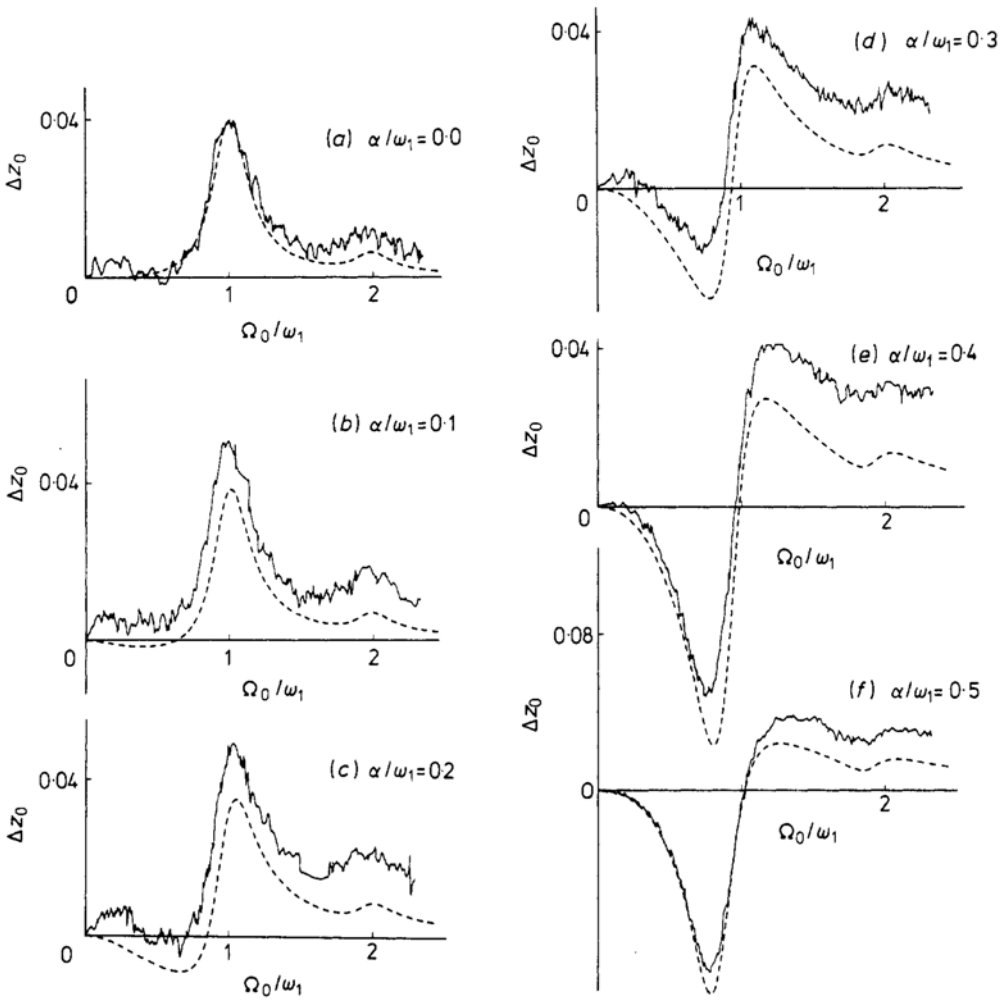

Figure 6. Differential fluorescence versus average Rabi frequency with $\omega_1/2\pi = 50$ MHz and $a = 0{\cdot}35 \pm 0{\cdot}04$. Broken lines: theory (numerical computation) (*a*) $\alpha = 0$; (*b*) $\alpha = 0{\cdot}1\omega_1$; (*c*) $\alpha = 0{\cdot}2\omega_1$; (*d*) $\alpha = 0{\cdot}3\omega_1$; (*e*) $\alpha = 0{\cdot}4\omega_1$; (*f*) $\alpha = 0{\cdot}5\omega_1$ (note scale change).

parametric resonances is strongly deformed in the range of detunings where they almost overlap. When $\alpha = 0{\cdot}5\omega_1$, the parametric resonances have almost completely disappeared and only the single-quantum ($n = 1$) and two-quantum ($n = 2$) resonances remain. The background signal due to hyperfine pumping increases with the detuning. This is a consequence of a less efficient two-state preparation, as the pumping beam is also detuned.

5.3. Standard resonances

The last series of curves (figure 7) was recorded by scanning the detuning (α) at different values of the average Rabi frequency Ω_0. Here the average fluorescence $\frac{1}{2}(1+z_m)$ is

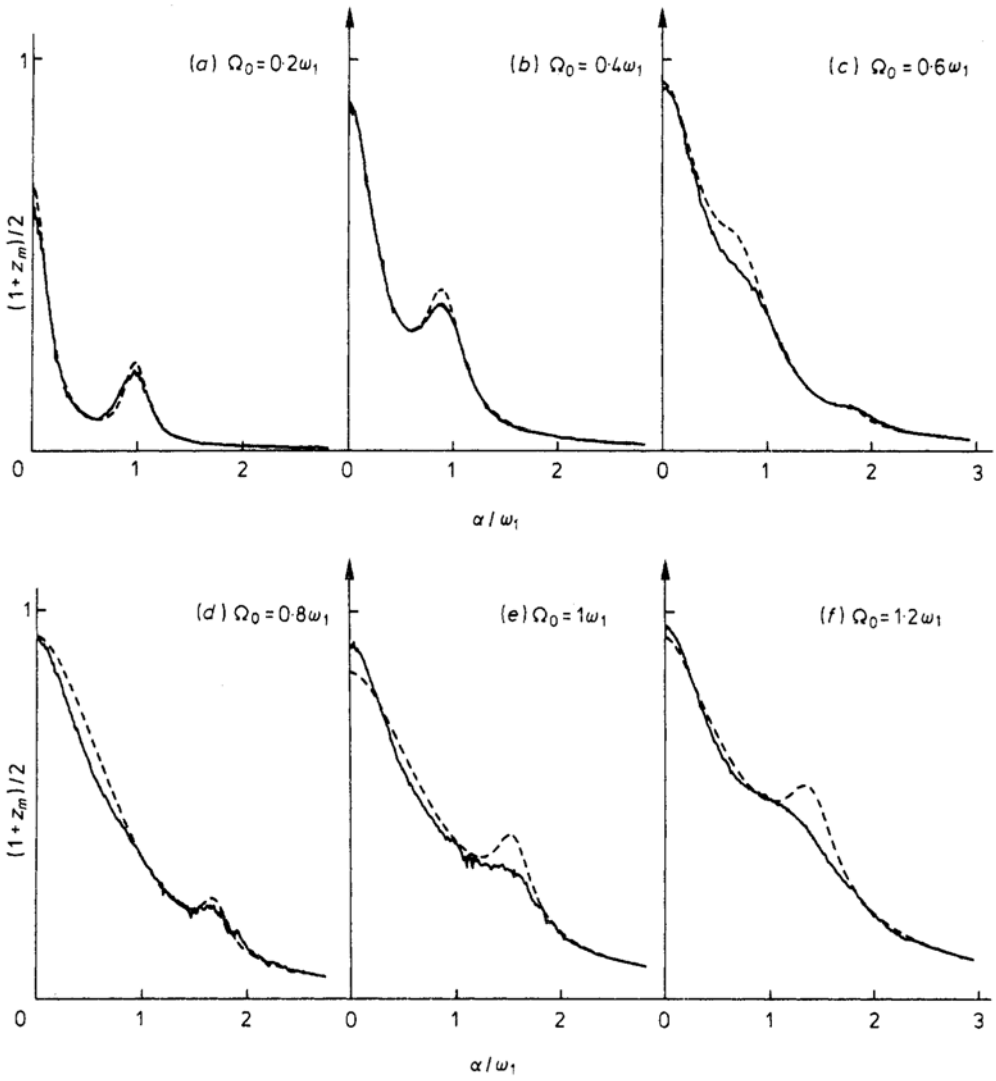

Figure 7. Average fluorescence versus detuning for $\omega_1/2\pi = 50$ MHz, $a = 1{\cdot}2$. Broken curves: theory (numerical computation) (*a*) $\Omega_0 = 0{\cdot}2\omega_1$; (*b*) $\Omega_0 = 0{\cdot}4\omega_1$; (*c*) $\Omega_0 = 0{\cdot}6\omega_1$; (*d*) $\Omega_0 = 0{\cdot}8\omega_1$; (*e*) $\Omega_0 = 1{\cdot}0\omega_1$; (*f*) $\Omega_0 = 1{\cdot}2\omega_1$.

displayed because it includes the resonance due to the carrier frequency ω_1 which does not appear in the differential fluorescence. The power broadening of the resonance is apparent and it agrees well with the theoretical shape. The additional resonances are brought in by the modulation. The single-quantum resonance due to the lower frequency sideband ($n = 1$, $\alpha/\omega_1 \simeq 1$) is seen on the curves in figures 7(a)–(c) and the two-quantum resonance ($n = 2$, $\alpha/\omega_1 \simeq 2$), which is forbidden when $\Omega_0 = 0$, appears for $\Omega_0 \geqslant 0{\cdot}6\omega_1$ (figures 7(c)–(f)). As expected its shift increases with Ω_0. Because a high modulation depth is required in order to observe these resonances, the beam amplitude stability was deteriorated due to thermal lensing in the modulator. As a consequence, the resonances whose position depends most strongly on Ω_0 are weakened and broadened ($n = 1$, figure 7(c); $n = 2$, figures 7(e) and (f)). Some evidence of the three-quantum resonance was obtained only for $\Omega_0 \simeq 0$ where its intensity is the greatest (figure 8).

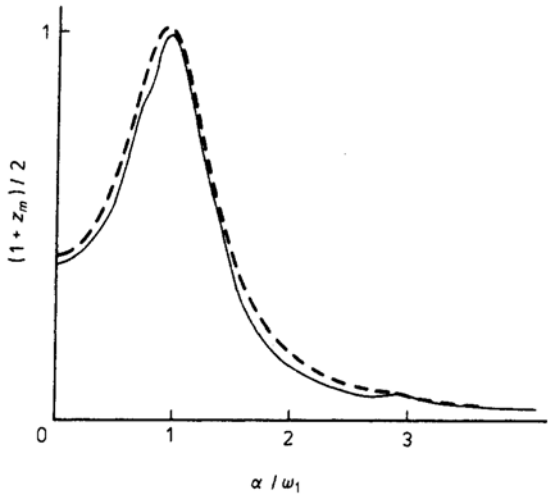

Figure 8. Average fluorescence versus detuning for $\omega_1/2\pi = 50$ MHz and $\Omega_0 = 0$. The curve shows the single-quantum and the three-quantum resonances.

6. Summary

We have studied the properties of the total fluorescent light scattered by two-level atoms in a strong modulated laser beam. Depending on whether the laser frequency is tuned to the atomic transition or not, two types of resonances can be observed, both of which have a known counterpart in magnetic resonance.

Parametric resonances occur with zero detuning. They are a consequence of the frequency-modulated Rabi flipping which is induced in the long-term atomic inversion by modulating the laser amplitude. The first two resonances have been observed. The amplitude of the first resonance increases quadratically with the modulation depth, as expected. Furthermore, the height of the resonance, which is dependent on the ratio of the two relaxation rates γ_T/γ_L, is consistent with the value of $\frac{1}{2}$ for spontaneous emission. The parametric resonance condition $\Omega_0 = n\omega_1$ gives a simple relation between the atomic dipole matrix element, the electric field of the laser and the

modulation frequency. It is worth noting that this relation could be applied to the measurement of unknown atomic dipole moments.

When the laser frequency is scanned around the atomic frequency, resonances involving three optical photons of frequency ω_L and $\omega_L \pm \omega_1$ ($\alpha = 2\omega_1$ and $3\omega_1$) have been observed in addition to the single-photon resonances ($\alpha = 0$ and ω_1). Their positions and intensities have been found to be in reasonable agreement with theoretical predictions despite difficulties in producing a stable beam with the required high modulation depth.

Acknowledgments

This work was initiated under the direction of Professor P Cornaz and benefited from his suggestions and his constant interest. I am greatly indebted to him for his stimulating and generous advice. I also wish to acknowledge many helpful discussions with Professor P R Fontana, and thank Professor S Feneuille for his interest in this experiment. Support from the Swiss National Science Foundation is gratefully acknowledged.

References

Abate J A 1974 *Opt. Commun.* **10** 269–72
Aleksandrov E B, Konstantinov O V, Perel V I and Khodovoi V A 1964 *Sov. Phys.–JETP* **18** 345–50
Allen L and Eberly J H 1975 *Optical Resonance and Two-Level Atoms* (New York: Wiley)
Armstrong L and Feneuille S 1975 *J. Phys. B: Atom. Molec. Phys.* **8** 546–51
Chapman G D and Series G W 1970 *J. Phys. B: Atom. Molec. Phys.* **3** 72–83
Citron M L, Gray H R, Gabel C W and Stroud C R 1977 *Phys. Rev.* A **16** 1507–12
Dagenais M and Mandel L 1978 *Phys. Rev.* A **18** 2217–28
Favre C and Geneux E 1964 *Phys. Lett.* **8** 190–2
Feneuille S, Schweighofer M G and Oliver G 1976 *J. Phys. B: Atom. Molec. Phys.* **9** 2003–9
Feynman R, Hellwarth R W and Vernon F L 1957 *J. Appl. Phys.* **28** 49–52
Fontana P R and Thomann P 1976 *Phys. Rev.* A **13** 1512–9
Grynberg G, Dupont-Roc J, Haroche S and Cohen-Tannoudji C 1973 *J. Physique* **34** 523–58
Haroche S 1971 *Ann. Phys., Paris* **6** 4–6
Hartig W, Rasmussen W, Schieder R and Walther H 1976 *Z. Phys.* A **278** 205–10
McClean W A and Swain S 1976 *J. Phys. B: Atom. Molec. Phys.* **9** 2011–5
Mollow B R and Miller M M 1969 *Ann. Phys., NY* **52** 464–78
Nakayama S and Ogawa T 1976 *J. Phys. Soc. Japan* **41** 950–7
Polonsky N and Cohen-Tannoudju C 1965 *C.R. Acad. Sci., Paris* **260** 5231–4
Schuda F, Stroud C R and Hercher M 1974 *J. Phys. B: Atom. Molec. Phys.* **7** L198–202
Thomann P, Chatelain P, Cornaz P and Geneux E 1974 *Helv. Phys. Acta* **47** 57–61
Thomann P 1975 *Proc. 7th EGAS Conference, Grenoble*
—— 1976 *J. Phys. B: Atom. Molec. Phys.* **9** 2411–9
Wilking S 1963 *Z. Phys.* **173** 490–508
Winter J M 1959 *Ann. Phys., Paris* **4** 745–811
Wu F, Grove R E and Ezekiel S 1975 *Phys. Rev. Lett.* **35** 1426–29
Yabuzaki T, Murakami Y and Ogawa T 1976 *J. Phys. B: Atom. Molec. Phys.* **9** 9–19